Geophys. J. Int. (2010) **181,** 577–590 doi: 10.1111/j.1365-246X.2010.04536.x

Stability of the high-order finite elements for acoustic or elastic wave propagation with high-order time stepping

Jonás D. De Basabe and Mrinal K. Sen

The Institute for Geophysics, John A. and Katherine G. Jackson School of Geosciences, The University of Texas at Austin, 10100 *Burnet Road,* R2200 *Austin,* TX 78758*, USA. E-mail: debasabe@alumni.utexas.net*

Accepted 2010 January 20. Received 2010 January 20; in original form 2009 September 2

SUMMARY

We investigate the stability of some high-order finite element methods, namely the spectral element method and the interior-penalty discontinuous Galerkin method (IP-DGM), for acoustic or elastic wave propagation that have become increasingly popular in the recent past. We consider the Lax-Wendroff method (LWM) for time stepping and show that it allows for a larger time step than the classical leap-frog finite difference method, with higher-order accuracy. In particular the fourth-order LWM allows for a time step 73 per cent larger than that of the leap-frog method; the computational cost is approximately double per time step, but the larger time step partially compensates for this additional cost. Necessary, but not sufficient, stability conditions are given for the mentioned methods for orders up to 10 in space and time. The stability conditions for IP-DGM are approximately 20 and 60 per cent more restrictive than those for SEM in the acoustic and elastic cases, respectively.

Key words: Numerical solutions; Numerical approximations and analysis; Computational seismology; Wave propagation.

1 INTRODUCTION

The numerical propagation of acoustic or elastic waves is a fundamental problem in many areas of science, engineering and industry. Applications are readily found in, but certainly not limited to, geophysics, acoustics, electromagnetics and elastodynamics. Numerical methods to accurately simulate the wave equation are being constantly developed and applied with increasing levels of sophistication. Nevertheless, often the accuracy and stability of these methods is poorly understood.

Particularly, in seismic modelling, there has recently been an increased interest in the high-order Finite Element Methods (FEM) (Seriani & Priolo 1994; Komatitsch & Vilotte 1998; Cohen 2002; Komatitsch *et al.* 2002; Chung & Engquist 2006; Grote *et al.* 2006; Käser & Dumbser 2006). These methods offer more geometrical flexibility and better control on the accuracy, compared to the traditional Finite Difference Methods (FDM). We focus on two such methods: The spectral element method (SEM) and the Interior-Penalty Discontinuous Galerkin Method (IP-DGM). We have discussed in our previous papers the accuracy, in terms of grid dispersion, for SEM (De Basabe & Sen 2007) and for IP-DGM (De Basabe *et al.* 2008). Here we elaborate further on the stability of these methods coupled with the Lax-Wendroff Method (LWM) for time stepping, which includes the leap-frog FDM as the lowest-order case. We derive specific stability bounds for the size of the time step with respect to the size of the elements and the maximum velocity. The stability analysis considers square elements in 2-D and is based on the ideas presented in Cohen (2002).

The classical approach to solve a second-order initial value problem is to use the Newmark method (Hughes 2000). The leap-frog Finite Difference Method (FDM) is a special case of this method that is second-order accurate, explicit and conditionally stable. This is the most popular time-stepping scheme in seismic modelling (Komatitsch & Tromp 1999; Chaljub *et al.* 2007; Cohen 2002; Grote *et al.* 2006). As noted by Dablain (1986), Cohen (2002), Gilbert & Joly (2008) and Diaz & Grote (2009), FDM can be generalized to obtain higher-order accuracy using a procedure analogous to the one used by Lax & Wendroff (1964). The advantage of this approach is that it does not require any modification of the wave equation and therefore existent codes that use FDM can be easily modified to use a higher-order LWM. Other high-order methods proposed for the discretization in time are the Runge–Kutta method (Cockburn & Shu 1989; Kubatko *et al.* 2007), the rapid expansion method (Tal-Ezer 1986; Kosloff *et al.* 1989), and the symplectic method (Simo *et al.* 1992; Tarnow & Simo 1994; Nissen-Meyer *et al.* 2008). A comparison of these methods is beyond the scope of this paper.

The remainder of this paper is organized as follows: In Section 2 we briefly describe the numerical methods under consideration. Section 3 contains the formulation of the grid dispersion and stability analysis and the stability conditions. In Section 4 we show the results of some numerical examples, and finally in Section 5 we summarize the conclusions.

2 DISCRETIZATIONS IN SPACE AND TIME OF THE WAVE EQUATION

This section summarizes the discretizations of the acoustic and elastic wave equations using the numerical methods under consideration, namely SEM, IP-DGM and LWM. The wave propagation phenomenon is modelled by the equation of motion, which is given by (using Einstein's summation convention)

$$\rho\partial_{tt}u_i = \partial_j\sigma_{ij} + f_i \quad \text{in} \quad \Omega\times(0,T] \quad i,j=1,\ldots,d, \tag{1}$$

where d is the number of physical dimensions (2 or 3), $\Omega\subset\mathbb{R}^d$ is the physical domain, $(0,T]$ is the time domain, u_i is the displacement vector, σ_{ij} is the stress tensor, and the source is described by the force vector f_i. The shorthand notation $\partial_l u_k = \partial u_k/\partial x_l$ is used in the above equation. The stress tensor can be written as a function of the displacement using the generalized Hooke's Law. In an isotropic medium, it is given by

$$\sigma_{ij}(\boldsymbol{u}) = \lambda\partial_k u_k\delta_{ij} + \mu(\partial_i u_j + \partial_j u_i), \tag{2}$$

where λ and μ are the Lamé parameters and are assumed to be varying in space in a heterogeneous medium, and δ_{ij} is the Kronecker's delta.

In an acoustic medium $\mu = 0$, thus the Hooke's law is simplified to

$$\sigma_{ij} = \lambda\partial_k u_k\delta_{ij} = \delta_{ij}p, \tag{3}$$

where p is the pressure field. Substituting in the equation of motion, dividing by the density, taking the divergence on both sides of the equation and prescribing suitable boundary and initial conditions, the acoustic wave equation is given by

$$\begin{aligned}
\lambda^{-1}\partial_{tt}p - \partial_i\rho^{-1}\partial_i p &= \tilde{f} \quad && \text{in} \quad \Omega\\
p &= 0 && \text{on} \quad \Gamma_D\\
\rho^{-1}\partial_i p\, n_i &= 0 && \text{on} \quad \Gamma_N\\
p = \partial_t p &= 0 && \text{for} \quad t=0
\end{aligned} \tag{4}$$

where $\tilde{f} = \partial_i\rho^{-1}f_i$, $\partial\Omega$ is the boundary of Ω, Γ_D and Γ_N are the subsets of the boundary where Dirichlet and Neumann boundry conditions are applied, respectively, and satisfy $\Gamma_D\cup\Gamma_N = \partial\Omega$, $\Gamma_D\cap\Gamma_N = \emptyset$, and n_i, $i=1,\ldots,d$, is a unit vector outward normal to $\partial\Omega$.

The elastic wave equation in an isotropic heterogeneous medium is obtained by substituting Hooke's law in the equation of motion, and is given by

$$\begin{aligned}
\rho\partial_{tt}u_i - \partial_i\lambda\partial_j u_j - \partial_j\mu(\partial_j u_i + \partial_i u_j) &= f_i \quad && \text{in} \quad \Omega\\
u_i &= 0 && \text{on} \quad \Gamma_D\\
\tau_i(\boldsymbol{u}) &= 0 && \text{on} \quad \Gamma_N\\
u_i = \partial_t u_i &= 0 && \text{for} \quad t=0,
\end{aligned} \tag{5}$$

where τ_i is the traction vector, given in the isotropic case by

$$\tau_i(\boldsymbol{u}) = \sigma_{ij}(\boldsymbol{u})n_j = \lambda\partial_k u_k n_i + \mu(\partial_i u_j + \partial_j u_i)n_j. \tag{6}$$

We have prescribed, for completeness, homogeneous boundary and initial conditions for eqs (4) and (5) but the analysis is independent of these since it is based on the von Neumann method and assumes an unbounded domain. In the following we focus for succinctness on the 2-D isotropic case.

2.1 Spectral element method

SEM, originally developed for fluid dynamics (Patera 1984), has been successfully applied to the wave equation, addressing the efficiency issues of FEM and providing better accuracy than FDM and more geometrical flexibility. This method was first implemented for the acoustic wave equation in the mid 1990's (Seriani & Priolo 1994; Tordjman *et al.* 1994; Tordjman 1995). The method was introduced to elastic wave propagation in the late 1990's in Komatitsch & Vilotte (1998), and it quickly gained tremendous credibility within the seismological community (Komatitsch & Tromp 1999, 2002; Priolo 2001; Komatitsch *et al.* 2005; Chaljub *et al.* 2007). The main characteristic of SEM is that it uses high-order basis functions, with the advantage that a lower sampling ratio can be used, typically between 4 and 5 nodes per wavelength. The mass matrix can be diagonalized by using the Gauss–Lobatto–Legendre (GLL) nodes for the distribution of the nodes inside the elements and the GLL quadrature rules for the approximation of its entries. The use of the GLL nodes and quadrature rules is tantamount to mass lumping, with the advantage that it preserves the accuracy.

We present a brief description of SEM in this section for completeness; a detailed description can be found in Komatitsch & Tromp (1999) and Cohen (2002). The first step in a finite element approximation is to derive the weak, or variational, formulations of eqs (4) and (5). The weak formulation is then discretized by introducing an approximation for the pressure or displacement in a finite-dimensional subspace to obtain a linear system of ordinary differential equations. The weak formulations and discretizations given below are applicable to FEM, the only difference for SEM is that the focus is on high-order basis functions and that the nodes are typically not equispaced.

The weak formulation of the acoustic wave equation is obtained by multiplying eq. (4) by a test function, integrating over the domain and applying the Gauss divergence theorem, and is given by the following statement: Find $p\in X^C$ such that for all $v\in X^C$

$$\partial_{tt}\left(\lambda^{-1}p, v\right)_\Omega + B_\Omega(p,v) = \left(\tilde{f}, v\right)_\Omega. \tag{7}$$

where

$$(u,v)_\Omega = \int_\Omega uv\,\mathrm{d}x\,\mathrm{d}z, \tag{8}$$

$$B_E(p,v) = \int_E \rho^{-1}\nabla p\cdot\nabla v\,\mathrm{d}x\,\mathrm{d}z, \tag{9}$$

and $X^C = \{\varphi \mid \varphi\in H^1(\Omega), \varphi = 0 \text{ on } \Gamma_D\}$ is an infinite-dimensional space that contains the exact solution. Using eq. (7), the original PDE can be written as a system of ODEs by introducing a finite dimensional subspace $X_h^C\subset X^C$, with basis $\{\phi_i\}_{i=1}^n$. Substituting in eq. (7) for p the approximation $p_h\in X_h^C$ given by the linear combination

$$p_h(x,z,t) = P_j(t)\phi_j(x,z)\,, \tag{10}$$

where P_j are the coefficients of the FEM approximation p_h, and substituting for v each of the basis functions, yields

$$M_{ij}\partial_{tt}P_j + K_{ij}P_j = F_i, \tag{11}$$

where

$$M_{ij} = \left(\lambda^{-1}\phi_j, \phi_i\right)_\Omega, \tag{12}$$

$$K_{ij} = B_\Omega(\phi_j,\phi_i), \tag{13}$$

$$F_i = (\tilde{f}, \phi_i). \tag{14}$$

Usually in the FEM literature $\boldsymbol{M} = (M_{ij})$ is called the mass matrix and $\boldsymbol{K} = (K_{ij})$ is called the stiffness matrix. The ODE system (11) is called the continuous in time or semi-discrete form of eq. (7) because it has been discretized in space through the substitution of the basis functions but the time derivative remains.

The weak form of the elastic wave equation is given by the following statement: Find $\boldsymbol{u} \in \boldsymbol{X}^C = \{\boldsymbol{\varphi} \mid \boldsymbol{\varphi} \in \boldsymbol{H}^1(\Omega),\ \boldsymbol{\varphi} = 0 \text{ on } \Gamma_D\}$ such that for all $\boldsymbol{v} \in \boldsymbol{X}^C$

$$\partial_{tt}\,(\rho \boldsymbol{u}, \boldsymbol{v})_\Omega + \boldsymbol{B}_\Omega\,(\boldsymbol{u}, \boldsymbol{v}) = (\boldsymbol{f}, \boldsymbol{v})_\Omega\,, \tag{15}$$

where

$$(\boldsymbol{u}, \boldsymbol{v})_\Omega = \int_\Omega \boldsymbol{u} \cdot \boldsymbol{v}\ \mathrm{d}x\ \mathrm{d}z, \tag{16}$$

$$\boldsymbol{B}_E\,(\boldsymbol{u}, \boldsymbol{v}) = \int_E \Big(\lambda(\nabla \cdot \boldsymbol{u})(\nabla \cdot \boldsymbol{v}) + \mu(\nabla \boldsymbol{u} + \nabla \boldsymbol{u}^T) : \nabla \boldsymbol{v}\Big)\ \mathrm{d}x\ \mathrm{d}z, \tag{17}$$

and the double-dot product is defined as $\boldsymbol{A} : \boldsymbol{B} = A_{ij}B_{ij}$ for $\boldsymbol{A} = (A_{ij})$ and $\boldsymbol{B} = (B_{ij})$.

We can now use the weak formulation of the elastic wave equation to obtain a system of ODEs by introducing the finite dimensional subspace $\boldsymbol{X}_h^C = X_h^C \times X_h^C \subset \boldsymbol{X}^C$. Substituting for $\boldsymbol{u}$ the approximation $\boldsymbol{u}_h \in \boldsymbol{X}_h^C$ given by the linear combination

$$\boldsymbol{u}_h(x, z, t) = \left(U_j^x(t)\phi_j(x, z)\ ,\ U_j^z(t)\phi_j(x, z)\right)^T\ , \tag{18}$$

where U_j^x and U_j^z are the coefficients of the FEM approximations to the horizontal and vertical displacement, respectively, and substituting $\boldsymbol{v} = (\phi_i, 0)^T$ yields the following system of equations

$$M_{ij}\partial_{tt}U_j^x + K_{ij}^1 U_j^x + K_{ij}^2 U_j^z = F_i^x. \tag{19}$$

Similarly, substituting $\boldsymbol{v} = (0, \phi_i)^T$, yields

$$M_{ij}\partial_{tt}U_j^z + K_{ij}^3 U_j^x + K_{ij}^4 U_j^z = F_i^z, \tag{20}$$

where the matrices in eqs (19) and (20) are given by

$$M_{ij} = (\rho\phi_i, \phi_j)_\Omega, \tag{21}$$

$$K_{ij}^1 = \boldsymbol{B}_\Omega\big((\phi_j, 0)^T, (\phi_i, 0)^T\big), \tag{22}$$

$$K_{ij}^2 = \boldsymbol{B}_\Omega\big((0, \phi_j)^T, (\phi_i, 0)^T\big), \tag{23}$$

$$K_{ij}^3 = \boldsymbol{B}_\Omega\big((\phi_j, 0)^T, (0, \phi_i)^T\big), \tag{24}$$

$$K_{ij}^4 = \boldsymbol{B}_\Omega\big((0, \phi_j)^T, (0, \phi_i)^T\big), \tag{25}$$

$$F_i^x = (f_x, \phi_i)_\Omega, \tag{26}$$

$$F_i^z = (f_z, \phi_i)_\Omega, \tag{27}$$

and f_x and f_z are the x and z components of $\boldsymbol{f}$.

2.2 Discontinuous Galerkin Method

The Discontinuous Galerkin Method (DGM) is a generalization of FEM that allows for the approximating functions to be discontinuous at the element interfaces. The continuity is imposed weakly with some extra terms in the weak formulation. There are many different ways to weakly impose the continuity, which give rise to the many different formulations of the DGM (e.g. Bernacki *et al.* 2006; Käser & Dumbser 2006; Chung & Engquist 2006; Grote *et al.* 2006). In the following we focus on the interior-penalty, or primal, formulations of this method. See Arnold *et al.* (2001) for an overview of other formulations and references in De Basabe *et al.* (2008) for other DGMs that have been applied to acoustic or elastic wave propagation. We give in this section a brief introduction to the method for completeness, see Rivière (2008) for more details.

The interior-penalty weak formulation of the acoustic wave equation is given by the following statement: Find $p \in X^D = \left\{\varphi \,|\, \varphi \in H^1(E)\ \forall\ E \in \Omega_h,\ \varphi = 0 \text{ on } \Gamma_D\right\}$ such that for all $v \in X^D$

$$\sum_{E\in\Omega_h}\Big(\left(\lambda^{-1}\partial_{tt}p, v\right)_E + B_E(p, v)\Big) + \sum_{\gamma\in\Gamma_h} J_\gamma(p, v; S, R) = \sum_{E\in\Omega_h}(\tilde{f}, v)_E \tag{28}$$

where Ω_h is the set of elements that discretize Ω, Γ_h is the set of all element interfaces, and

$$\begin{aligned} J_\gamma(p, v; S, R) = &-\int_\gamma \{\rho^{-1}\nabla p \cdot \boldsymbol{n}^\gamma\}[v]\ d\gamma \\ &+ S\int_\gamma \{\rho^{-1}\nabla v \cdot \boldsymbol{n}^\gamma\}[p]\ d\gamma \\ &+ R\int_\gamma \{\rho^{-1}\}[p][v]\ d\gamma \quad \forall\gamma \in \Gamma_h. \end{aligned} \tag{29}$$

The parameter R in eq. (29) is the penalty, and S is a parameter that takes the values 0, 1 or -1 depending on the particular formulation of IP-DGM:

(1) $S = 0$ for the Incomplete Interior Penalty Galerkin (IIPG) (Dawson *et al.* 2004),
(2) $S = -1$ for the Symmetric Interior Penalty Galerkin (SIPG) (Darlow 1980; Grote *et al.* 2006) and
(3) $S = 1$ for the Non-symmetric Interior Penalty Galerkin (NIPG) (Rivière *et al.* 1999; Rivière *et al.* 2001).

To solve for the pressure in eq. (28), a subspace $X_h^D \subset X^D$ is introduced by defining a finite number of basis functions $\{\phi_i^E\}_{i=1}^m$ in element E for all $E \in \Omega_h$. Basis functions for IP-DGM that are suitable for wave propagation have been discussed in De Basabe *et al.* (2008), and are summarized in Appendix A. The analysis will take advantage of these basis functions being defined element wise, but for the purposes of this section, a global enumeration of the basis functions will be introduce here $\varphi_j = \phi_i^e$, where $j = i + em$, $e = 0, \ldots, N_e - 1$, and N_e is the total number of elements in Ω_h. With this numbering of the basis functions, a linear system like that in eq. (11) is obtained, where

$$M_{ij} = \sum_{E\in\Omega_h}(\lambda^{-1}\varphi_j, \varphi_i)_E, \tag{30}$$

$$K_{ij} = \sum_{E\in\Omega_h} B_E(\varphi_j, \varphi_i) + \sum_{\gamma\in\Gamma_h} J_\gamma(\varphi_j, \varphi_i; S, R), \tag{31}$$

$$F_i = \sum_{E\in\Omega_h}(\tilde{f}, \varphi_i)_E. \tag{32}$$

The interior-penalty weak formulation of the elastic wave equation is given by the following statement: Find $\boldsymbol{u} \in \boldsymbol{X}^D =$

$\{\varphi \,|\, \varphi \in \boldsymbol{H}^1(E)\ \forall\ E \in \Omega_h,\ \boldsymbol{\varphi} = 0 \text{ on } \Gamma_D\}$ such that for all $\boldsymbol{v} \in \boldsymbol{X}^D$

$$\sum_{E\in\Omega_h}\Big((\rho\partial_{tt}\boldsymbol{u},\boldsymbol{v})_E + \boldsymbol{B}_E(\boldsymbol{u},\boldsymbol{v})\Big) + \sum_{\gamma\in\Gamma_h}\boldsymbol{J}_\gamma(\boldsymbol{u},\boldsymbol{v};S,R) = \sum_{E\in\Omega_h}(\boldsymbol{f},\boldsymbol{v})_E \tag{33}$$

where $\boldsymbol{v}$ is a vector test function and

$$\boldsymbol{J}_\gamma(\boldsymbol{u},\boldsymbol{v};S,R) = -\int_\gamma \{\tau_i(\boldsymbol{u})\}[v_i]\,d\gamma + S\int_\gamma \{\tau_i(\boldsymbol{v})\}[u_i]\,d\gamma + R\int_\gamma \{\lambda+2\mu\}[u_i][v_i]\,d\gamma. \tag{34}$$

The parameters R and S in eq. (34) are defined as in eq. (28).

Introducing the subspace $\boldsymbol{X}_h^D = X_h^D \times X_h^D \subset \boldsymbol{X}^D$ and substituting in eq. (33) the test function and the displacement by linear combinations of the basis functions, yields a system of ordinary differential equations like the one in eqs (19) and (20), where

$$M_{ij} = \sum_{E\in\Omega_h}(\rho\varphi_j,\varphi_i)_E, \tag{35}$$

$$K_{ij}^1 = \sum_{E\in\Omega_h}\boldsymbol{B}_E\big((\varphi_j,0)^T,(\varphi_i,0)^T\big) + \sum_{\gamma\in\Gamma_h}\boldsymbol{J}_\gamma\big((\varphi_j,0)^T,(\varphi_i,0)^T\big), \tag{36}$$

$$K_{ij}^2 = \sum_{E\in\Omega_h}\boldsymbol{B}_E\big((0,\varphi_j)^T,(\varphi_i,0)^T\big) + \sum_{\gamma\in\Gamma_h}\boldsymbol{J}_\gamma\big((0,\varphi_j)^T,(\varphi_i,0)^T\big), \tag{37}$$

$$K_{ij}^3 = \sum_{E\in\Omega_h}\boldsymbol{B}_E\big((\varphi_j,0)^T,(0,\varphi_i)^T\big) + \sum_{\gamma\in\Gamma_h}\boldsymbol{J}_\gamma\big((\varphi_j,0)^T,(0,\varphi_i)^T\big), \tag{38}$$

$$K_{ij}^4 = \sum_{E\in\Omega_h}\boldsymbol{B}_E\big((0,\varphi_j)^T,(0,\varphi_i)^T\big) + \sum_{\gamma\in\Gamma_h}\boldsymbol{J}_\gamma\big((0,\varphi_j)^T,(0,\varphi_i)^T\big), \tag{39}$$

$$F_i^x = \sum_{E\in\Omega_h}(f_x,\varphi_i)_E, \tag{40}$$

$$F_i^z = \sum_{E\in\Omega_h}(f_z,\varphi_i)_E. \tag{41}$$

2.3 Lax-Wendroff method

LWM (Lax & Wendroff 1964) aims to obtain formally a higher-order accuracy in time without demanding to save many time steps. It was introduced to seismic modelling in Dablain (1986) in the context of Finite Differences and later used in Cohen (2002) and Jund & Salmon (2007) in the context of SEM and in Käser & Dumbser (2006) in the context of DGM (called the ADER approach in this case). This approach is based on a Taylor expansion in time of the wavefield and a substitution of the high-order time derivatives by matrix operations. In this section we summarize the method as applied to second-order systems, as opposed to the first order systems considered, for example, in Lax & Wendroff (1964), Käser & Dumbser (2006) or Jund & Salmon (2007).

This strategy is applicable to either SEM or IP-DGM and to the acoustic or elastic formulations. The following notation will be used for the linear system in order to emphasize the generality of the strategies:

$$\begin{aligned}\boldsymbol{A}\partial_{tt}\boldsymbol{\chi} &= -\boldsymbol{B}\boldsymbol{\chi} + \boldsymbol{f},\\ \boldsymbol{\chi}(0) &= \partial_t\boldsymbol{\chi}(0) = 0,\end{aligned} \tag{42}$$

where, in the acoustic case, $\boldsymbol{\chi}$ contains the coefficients of the pressure field, $\boldsymbol{A}$ is the mass matrix as defined in eqs (12) or (30), and $\boldsymbol{B}$ is the stiffness matrix as defined in eqs (13) or (31). In the elastic case, $\boldsymbol{\chi}$ contains the coefficients of the two components of displacement, and $\boldsymbol{A}$ and $\boldsymbol{B}$ are the block matrices given by

$$\boldsymbol{A} = \begin{pmatrix}\boldsymbol{M} & \boldsymbol{0}\\ \boldsymbol{0} & \boldsymbol{M}\end{pmatrix}, \tag{43}$$

$$\boldsymbol{B} = \begin{pmatrix}\boldsymbol{K}^1 & \boldsymbol{K}^2\\ \boldsymbol{K}^3 & \boldsymbol{K}^4\end{pmatrix}, \tag{44}$$

where $\boldsymbol{M}$ and $\boldsymbol{K}^i$, $i = 1,\ldots,4$, are the mass and stiffness matrices as defined in eqs (21)–(25) or (35)–(39).

The application of the LWM to eq. (42) has been described in Cohen (2002) and Dablain (1986). It is interesting to note that this method usually bears other names when it is applied to second order systems, for example, in Cohen (2002) it is called the modified equation approach. Nevertheless, due to the important similarities with the original formulation, it is suitable to regard this as a LWM. The first part of this method is to obtain an expression that allows the substitution of the higher-order time derivatives by matrix operation, which is given by the following theorem.

Theorem 1. The $2k$th order time derivative of $\boldsymbol{\chi}$ is given by

$$\partial_t^{2k}\boldsymbol{\chi} = (-\boldsymbol{A}^{-1}\boldsymbol{B})^k\boldsymbol{\chi} + \sum_{l=0}^{k-1}(-\boldsymbol{A}^{-1}\boldsymbol{B})^l\boldsymbol{A}^{-1}\partial_t^{2(k-l-1)}\boldsymbol{f}. \tag{45}$$

**Proof.* Proceeding by induction, taking $k = 1$ yields exactly eq. (42). Taking now $k+1$ and using eqs (42) and (45) yields

$$\begin{aligned}\partial_t^{2k+2}\boldsymbol{\chi} &= \partial_t^2(\partial_t^{2k}\boldsymbol{\chi})\\ &= \partial_t^2\left((-\boldsymbol{A}^{-1}\boldsymbol{B})^k\boldsymbol{\chi} + \sum_{l=0}^{k-1}(-\boldsymbol{A}^{-1}\boldsymbol{B})^l\boldsymbol{A}^{-1}\partial_t^{2(k-l-1)}\boldsymbol{f}\right)\\ &= (-\boldsymbol{A}^{-1}\boldsymbol{B})^k\partial_t^2\boldsymbol{\chi} + \sum_{l=0}^{k-1}(-\boldsymbol{A}^{-1}\boldsymbol{B})^l\boldsymbol{A}^{-1}\partial_t^{2(k-l)}\boldsymbol{f}\\ &= (-\boldsymbol{A}^{-1}\boldsymbol{B})^{k+1}\boldsymbol{\chi} + (-\boldsymbol{A}^{-1}\boldsymbol{B})^k\boldsymbol{A}^{-1}\boldsymbol{f}\\ &\quad + \sum_{l=0}^{k-1}(-\boldsymbol{A}^{-1}\boldsymbol{B})^l\boldsymbol{A}^{-1}\partial_t^{2(k-l)}\boldsymbol{f}\\ &= (-\boldsymbol{A}^{-1}\boldsymbol{B})^{k+1}\boldsymbol{\chi} + \sum_{l=0}^{k}(-\boldsymbol{A}^{-1}\boldsymbol{B})^l\boldsymbol{A}^{-1}\partial_t^{2(k-l)}\boldsymbol{f},\end{aligned}$$

which is eq. (45) for $k+1$. □

The second part of this method is to obtain a Taylor expansion for the time stepping. Evaluating the Taylor expansion of $\boldsymbol{\chi}$ at $t+\Delta t$ and $t-\Delta t$ yields

$$\boldsymbol{\chi}^{n+1} = \boldsymbol{\chi}^n + \Delta t\,\partial_t\boldsymbol{\chi}^n + \frac{\Delta t^2}{2}\partial_t^2\boldsymbol{\chi}^n + \frac{\Delta t^3}{3!}\partial_t^3\boldsymbol{\chi}^n + \ldots, \tag{46}$$

$$\boldsymbol{\chi}^{n-1} = \boldsymbol{\chi}^n - \Delta t\,\partial_t\boldsymbol{\chi}^n + \frac{\Delta t^2}{2}\partial_t^2\boldsymbol{\chi}^n - \frac{\Delta t^3}{3!}\partial_t^3\boldsymbol{\chi}^n + \ldots, \tag{47}$$

where $\boldsymbol{\chi}^n = \boldsymbol{\chi}\ (n\Delta t)$. Upon addition of the above equations the odd-order terms mutually cancel, to obtain

$$\boldsymbol{\chi}^{n+1} - 2\boldsymbol{\chi}^n + \boldsymbol{\chi}^{n-1} = 2\sum_{k=1}^{N} \frac{\Delta t^{2k}}{(2k)!}\partial_t^{2k}\boldsymbol{\chi}^n + O(\Delta t^{2N}). \tag{48}$$

Note that the above equation requires only even-order derivatives. These can be substituted by matrix multiplications using eq. (45) to obtain

$$\boldsymbol{\chi}^{n+1} - 2\boldsymbol{\chi}^n + \boldsymbol{\chi}^{n-1} = 2\sum_{k=1}^{N} \frac{\Delta t^{2k}}{(2k)!}\left((-\boldsymbol{A}^{-1}\boldsymbol{B})^k\boldsymbol{\chi}^n + \sum_{l=0}^{k-1}(-\boldsymbol{A}^{-1}\boldsymbol{B})^l\boldsymbol{A}^{-1}\partial_t^{2(k-l-1)}\boldsymbol{f}\right) + O(\Delta t^{2N}). \tag{49}$$

Given $\boldsymbol{\chi}^n$ and $\boldsymbol{\chi}^{n-1}$, $\boldsymbol{\chi}^{n+1}$ can be readily calculated using eq. (49). This method includes the leap-frog FDM as the special case when $N = 1$, therefore in this sense it is a higher-order generalization of FDM. The limitation of this approach is that it cannot be directly applied when there is a first-order time derivative in eq. (42). First order time derivatives can be accommodated by writing eq. (42) as a first order system using a velocity–stress or velocity–displacement formulation and using the classical LWM (Lax & Wendroff 1964).

3 PLANE WAVE ANALYSIS

The grid dispersion and stability analyses are the most important analytical tools that help determine the simulation parameters for the numerical propagation of acoustic or elastic waves. This section presents the analysis of SEM and IP-DGM for acoustic and elastic wave propagation. Particular attention will be devoted to allow for non-equispaced nodes and high-order basis functions. It is a continuation of our previous work (De Basabe & Sen 2007; De Basabe *et al.* 2008), where we focused on the accuracy in terms of grid dispersion, and here the focus is on stability.

The analysis is based on the von Neumann method (Mitchell & Griffiths 1980; Hughes 2000), which assumes a plane wave propagating through the finite-element domain. The plane wave assumption leads to a generalized eigenvalue formulation that is originally large, proportional to the number of nodes in the finite element mesh. However, with some assumptions, it can be reduced to a smaller one, proportional to the number of nodes inside one element.

Since the goal of the analysis is to derive the stability condition, to have a manageable set of parameters the analysis makes several assumptions about the medium and the finite-element mesh. The analysis assumes that the medium is isotropic, homogeneous, unbounded and source free, that the finite-element mesh is periodic, and that the elements are square with sides parallel to the coordinate axis and with tensor product basis functions. These are ubiquitous assumptions whenever a plane wave analysis is sought (Mullen & Belytschko 1982; Marfurt 1984; Hu *et al.* 1999; Cohen 2002; Zyserman *et al.* 2003; Ainsworth 2004a;b; Ainsworth *et al.* 2006; De Basabe & Sen 2007; De Basabe *et al.* 2008). In practice these assumptions are not expected to be satisfied, nevertheless the results from an analysis based on these assumptions can provide valuable information to determine the discretization parameters for a numerical experiment.

We now proceed to derive a generalized eigenvalue problem which eigenvalues are related to the grid dispersion and stability of the methods in question. The starting point is the classical leap-frog method for time stepping, it will be shown in the following section how this applies to the higher-order LWM. Introducing the simplifying assumptions in eq. (42) yields

$$\boldsymbol{\mathcal{A}}\partial_{tt}\boldsymbol{\chi} = -\alpha^2\boldsymbol{\mathcal{B}}\boldsymbol{\chi}, \tag{50}$$

where α is the *P*-wave velocity, and $\boldsymbol{\mathcal{A}}$ and $\boldsymbol{\mathcal{B}}$ are as in eq. (42) but with simplifications because a homogeneous medium is now assumed. The expressions for the simplified mass and stiffness matrices are given in Appendix B. If we assume that the solution is a plane wave then

$$\chi_j(t) = c_j e^{\mathrm{i}(\boldsymbol{k}\cdot\boldsymbol{x}_j - \omega_h t)}, \tag{51}$$

where c_j is an arbitrary constant, $\boldsymbol{k}$ is the wavenumber, $\boldsymbol{x}_j$ contains the jth node coordinates, and ω_h is the numerical angular frequency. Substituting the plane wave solution into eq. (50) yields

$$\Lambda\boldsymbol{\mathcal{A}}\boldsymbol{c} = \boldsymbol{\mathcal{B}}\boldsymbol{c}, \tag{52}$$

where the eigenvalue takes the form

$$\Lambda = \frac{4}{\alpha^2\Delta t^2}\sin^2\left(\frac{\omega_h\Delta t}{2}\right), \tag{53}$$

for the leap-frog FDM case. The order of the above eigenvalue problem depends on the number of degrees of freedom in a particular discretization. We have described in detail in our previous work (De Basabe & Sen 2007; De Basabe *et al.* 2008) how to reduce the eigenvalue problem to one of order proportional to the degrees of freedom inside one element, denoted by

$$\Lambda\tilde{\boldsymbol{A}}\boldsymbol{c} = \tilde{\boldsymbol{B}}\boldsymbol{c}, \tag{54}$$

where $\tilde{\boldsymbol{A}}$ and $\tilde{\boldsymbol{B}}$ are the so-called dynamic mass and stiffness matrices (see Appendix B). Finally, in order to derive the stability conditions, we compute the dynamic mass and stiffness matrices in the master element to factor out the size of the elements h, which yields the eigenvalue problem

$$\Lambda'\tilde{\boldsymbol{A}}\boldsymbol{c} = \tilde{\boldsymbol{B}}\boldsymbol{c}, \tag{55}$$

with eigenvalues

$$\Lambda' = \frac{4h^2}{\alpha^2\Delta t^2}\sin^2\left(\frac{\omega_h\Delta t}{2}\right). \tag{56}$$

3.1 Stability conditions

We now proceed to derive the stability conditions for SEM and IP-DGM and for the acoustic and elastic cases using the eigenvalues from the previous sections. We first consider the leap-frog FDM for time stepping and then generalize the results to LWM. For concreteness, the specific stability bounds for degrees 1 to 10 and an example on how to apply them in practice are given.

Let us consider the eigenvalues of eq. (55). Using the definition of the eigenvalues for the finite-difference in time case, eq. (56), yields

$$\frac{\mathrm{q}^2}{4}\Lambda' = \sin^2\frac{\omega_h\Delta t}{2} \leq 1, \tag{57}$$

where $\mathrm{q} = \alpha\Delta t/h$ is the *stability parameter*. Equivalently, the inequality (57) can be written as $\mathrm{q} \leq 2/\sqrt{\Lambda'}$. Note that Λ' is a function of the wavenumber through the dynamic mass and stiffness matrices (see Appendix B), and that the above inequality must be satisfied for all the eigenvalues and all the wavenumbers, thus the *stability condition* is given by

$$\mathrm{q} \leq \min_{1\leq j\leq \nu}\min_{0\leq\theta\leq 2\pi} 2\Lambda'_j(\theta)^{-1/2}, \tag{58}$$

Table 1. Upper bounds for the stability parameter in the acoustic case.

Degree	SEM	SIPG	IIPG	NIPG	Gauss	Legendre
1	0.709	0.408	0.408	0.353	0.288	0.288
2	0.288	0.182	0.166	0.152	0.163	0.100
3	0.164	0.108	0.0934	0.0831	0.103	0.0615
4	0.104	0.0725	0.0600	0.0522	0.0707	0.0404
5	0.0714	0.0520	0.0419	0.0359	0.0512	0.0289
6	0.0516	0.0391	0.0309	0.0262	0.0387	0.0216
7	0.0390	0.0305	0.0238	0.0200	0.0303	0.0168
8	0.0304	0.0244	0.0188	0.0157	0.0243	0.0135
9	0.0244	0.0200	0.0153	0.0127	0.0199	0.0110
10	0.0200	0.0167	0.0126	0.0105	0.0166	0.00921

Notes: The constants for SIPG, IIPG and NIPG are computed using the GLL basis functions. The last two columns correspond to SIPG using the Gauss and Legendre basis functions.

where θ is the incidence angle and ν is the number of eigenvalues, $\nu = \kappa^2$ for SEM and $\nu = (\kappa + 1)^2$ for IP-DGM in the acoustic case, and $\nu = 2\kappa^2$ for SEM and $\nu = 2(\kappa + 1)^2$ for IP-DGM in the elastic case, and κ is the polynomial degree of the basis functions in one side of the elements.

Necessary, but not sufficient, bounds for the stability parameter in the acoustic case for degrees from 1 to 10 are given in Table 1 using the GLL basis functions. Although theoretically these bounds are only necessary, our numerical experiments indicate that they are sufficient as well, i.e. the methods are stable below and unstable above these bounds. This results agree with those obtained by Fauqueux (2003). Note that the constants for SIPG are roughly 20 per cent smaller than those for SEM, and that IIPG and NIPG have more restrictive constants than those for SIPG. For completeness, the constants for SIPG using the Gauss and Legendre basis functions are shown in the last two columns (see Appendix A). The constants for the Gauss basis are slightly smaller than those for the GLL basis, and the ones for the Legendre basis are significantly smaller. Following Ainsworth *et al.* (2006), the penalty used for IP-DGM is $R = (\kappa + 1)(\kappa + 2)/(2\ |\gamma|)$, where $|\gamma|$ is the length of the face γ. The numerical experiments indicate that a smaller penalty yields inaccurate results. On the other hand, using a bigger penalty yields accurate results but more restrictive stability conditions.

In practice, the time step is often bounded, not by the size of the elements, but by the smaller space increment. In order to give the stability conditions that are readily useful for numerical simulations, we show in Table 2 the stability conditions for the *modified* stability parameter, given by

$$\mathrm{q}' = \frac{\alpha \Delta t}{\Delta x}, \tag{59}$$

where Δx is the smallest space increment.

Table 2. Upper bounds for the modified stability parameter q' in the acoustic case.

Degree	SEM	SIPG	IIPG	NIPG
1	0.709	0.408	0.408	0.353
2	0.577	0.365	0.333	0.305
3	0.593	0.393	0.338	0.301
4	0.604	0.420	0.347	0.302
5	0.608	0.443	0.357	0.306
6	0.608	0.461	0.364	0.309
7	0.608	0.476	0.371	0.312
8	0.607	0.488	0.376	0.314
9	0.607	0.498	0.381	0.316
10	0.607	0.506	0.384	0.318

Note: The constants for SIPG, IIPG and NIPG are computed using the GLL basis functions.

Table 3. Upper bounds for the stability parameter in the elastic case using $r = 1.41$.

Degree	SEM	SIPG	IIPG	NIPG
1	0.816	0.288	0.287	0.272
2	0.333	0.121	0.117	0.113
3	0.189	0.0683	0.0650	0.0622
4	0.120	0.0439	0.0413	0.0392
5	0.0823	0.0306	0.0286	0.0270
6	0.0595	0.0226	0.0210	0.0197
7	0.0449	0.0173	0.0161	0.0150
8	0.0350	0.0137	0.0127	0.0118
9	0.0281	0.0111	0.0103	0.00960
10	0.0230	0.00926	0.00852	0.00792

Note: The constants for SIPG, IIPG and NIPG are computed using the GLL basis functions.

The stability conditions for the elastic case are given in Table 3 using the GLL basis functions and $r = 1.41$, where $r = \alpha/\beta$ is the *P*- to *S*-wave velocity ratio; this choice of r gives the more restrictive stability conditions, the stability conditions for higher values of r are slightly larger. The constants for SIPG are roughly 60 per cent smaller than those for SEM, and IIPG and NIPG have constants slightly more restrictive than those for the SIPG. We have numerically tested the stability limits from Table 3 and found that they are up to 10 per cent higher than the actual stability limits for SEM, and for IP-DGM they are necessary and sufficient conditions. The stability conditions for the modified stability parameter are shown in Table 4. The penalty used for IP-DGM is $R = 2(\kappa + 1)(\kappa + 2)/(2\ |\gamma|)$. We have determined these penalties through extensive numerical experimentation; smaller penalties yield spurious reflections at the element interfaces and higher penalties yield more restrictive stability conditions.

The stability conditions given above are related to those for the LWM by very simple relations. Recall from last section that the time-stepping scheme of the LWM is based on the expression (ignoring the source term)

$$\boldsymbol{\chi}^{n+1} - 2\boldsymbol{\chi}^{n} + \boldsymbol{\chi}^{n-1} = 2\sum_{k=1}^{N} \frac{\Delta t^{2k}}{(2k)!} \left(-\boldsymbol{A}^{-1}\boldsymbol{B}\right)^{k} \boldsymbol{\chi}^{n}. \tag{60}$$

Table 4. Upper bounds for the modified stability parameter q' in the elastic case using $r = 1.41$.

Degree	SEM	SIPG	IIPG	NIPG
1	0.816	0.288	0.287	0.272
2	0.666	0.243	0.235	0.226
3	0.684	0.247	0.235	0.225
4	0.697	0.254	0.239	0.227
5	0.700	0.261	0.244	0.230
6	0.700	0.266	0.247	0.232
7	0.700	0.271	0.251	0.235
8	0.699	0.274	0.253	0.236
9	0.698	0.278	0.256	0.238
10	0.698	0.280	0.258	0.240

Note: The constants for SIPG, IIPG and NIPG are computed using the GLL basis functions.

Table 5. Constants for the stability of LWM.

N	Order	C_N
1	2	1
2	4	1.732
3	6	1.375
4	8	2.317
5	10	2.783

Introducing the simplifying assumptions and plane wave analysis, yields

$$2\sin^2\frac{\omega_h\Delta t}{2}=\sum_{k=1}^{N}\frac{-\mathrm{q}^{2k}}{(2k)!}\left(-\Lambda'\right)^k, \tag{61}$$

where Λ' are the same as above. The right-hand side is a polynomial in q of degree $2N$; for example, for $N=1$ we obtain eq. (57). In general, the stability parameter needs to satisfy

$$0\le\sum_{k=1}^{N}\frac{-\mathrm{q}^{2k}}{(2k)!}\left(-\Lambda'\right)^k\le 2. \tag{62}$$

To obtain the specific bounds for the stability parameter we define $y=q^2\,\Lambda'$ and solve the resulting polynomials. For $N=2$ we obtain the following inequality:

$$0\le\frac{y}{2}-\frac{y^2}{4!}\le 2. \tag{63}$$

The inequality on the right is satisfied for all y, but the inequality on the left requires that $0\le y\le 12$, or equivalently $\mathrm{q}\le 2\sqrt{3}/\sqrt{\Lambda'}$ (in agreement with Cohen 2002; Gilbert & Joly 2008). Similarly, for the higher-order schemes, we obtain $\mathrm{q}\le 2C_N/\sqrt{\Lambda'}$, where C_N is a constant that depends only on the order of the LWM, and its values are given in Table 5. As in the finite-difference case, the inequality needs to be satisfied for all the eigenvalues and all incidence angles, therefore the stability condition is

$$\mathrm{q}\le C_N\min_{1\le j\le v}\min_{0\le\theta\le 2\pi}2\Lambda'_j(\theta)^{-1/2}. \tag{64}$$

Note that the approximation order is $2N$, and that $N=1$ corresponds to the leap-frog FDM. Since the number of operations required are approximately N times those of the leap-frog scheme, the constants for the higher-order cases are not large enough to upset the extra cost (Cohen 2002). In particular, the 6th order method allow for a time step only 37 per cent larger than the 2nd order, but requires approximately 3 times as many operations. The fourth-order method is the one closest to optimal and the most useful in practice.

The stability constant for a given method, degree and order is given by the product of the corresponding constant in either Tables 1 or 3, and the one from Table 5. For example, for the fourth-degree acoustic SEM using the leap-frog FDM, the stability condition is given by $\mathrm{q}\le 0.104$. If the P-wave velocity and size of the elements are given by $\alpha=1.5\ \mathrm{km\,s^{-1}}$ and $h=0.04$ km, then the time step would be bounded by $\Delta t\le 0.0027$. If the fourth-order LWM is used for the time stepping instead, then $\Delta t\le 0.0027\times 1.732=0.0048$.

3.2 Grid dispersion

We now proceed to write grid-dispersion relations that include the effects of the discretizations in space and time. From eq. (61), we have that

$$\frac{\omega_h\Delta t}{2}=\sin^{-1}\sqrt{\frac{1}{2}\sum_{k=1}^{N}\frac{-\mathrm{q}^{2k}}{(2k)!}\left(-\Lambda'\right)^k}. \tag{65}$$

Substituting $\omega_h=2\pi\alpha_h\delta/h$, where $\delta=h/(\kappa L)$ is the sampling ratio averaged over the element, yields

$$\frac{\alpha_h}{\alpha}=\frac{1}{\pi\delta\mathrm{q}}\sin^{-1}\sqrt{\frac{1}{2}\sum_{k=1}^{N}\frac{-\mathrm{q}^{2k}}{(2k)!}\left(-\Lambda'_P\right)^k} \tag{66}$$

for the P-wave dispersion. Similarly, for the S-wave dispersion, we have

$$\frac{\beta_h}{\beta}=\frac{r}{\pi\delta\mathrm{q}}\sin^{-1}\sqrt{\frac{1}{2}\sum_{k=1}^{N}\frac{-\mathrm{q}^{2k}}{(2k)!}\left(-\Lambda'_S\right)^k}, \tag{67}$$

where Λ_P and Λ_S are the eigenvalues that correspond to the P and S waves, respectively, $\delta=h/\kappa L$ is the average sampling ratio, h is the size of one side of the elements and L is the wavelength. The above equation represents the rate of the numerical to the physical velocity thus a digression from unity indicate numerical error.

The numerical anisotropy introduced by the grid dispersion of the different methods is plotted in Figs 1–4. Note that in all the figures, due to the low numerical dispersion of the methods under consideration, the dispersion has been exaggerated by computing it for a large number of wavelengths. Fig. 1 shows the numerical dispersion of SEM using the lowest-order LWM and a time step given by 25 per cent, 50 per cent and 90 per cent of the stability conditions given in Table 3. Fig. 1(a) reveals that using a time step close to the stability limit introduces a dispersion that is approximately 20 per cent for 100 wavelengths and $\kappa=2$; Using a smaller time step helps decrease this numerical error. A similar observation applies for $\kappa=3$ and 4, and for IP-DGM (Fig. 2). We have used larger magnification factors for Fig. 2 than for Fig. 1 for visualization purposes, because the small time steps required by IP-DGM yield a smaller dispersion. Comparing Figs 1 and 2 with 3 and 4, respectively, reveals that it is advantageous to use the fourth-order LWM but no further improvements are observed for the higher order methods. Note in these figures that the curves for $N=2$ and 3 overlap those of the semi-discrete case and that all of them consider a time step that is 90 per cent of the stability limit (the curves for $N=1$ are exactly the same as the ones for 90 per cent in Figs 1 and 2).

4 EXAMPLES

We have numerically tested the stability of the methods and compared the accuracy of the synthetic seismograms for different sizes of the time step. For the numerical examples we consider the Lamb's problem (Lamb 1904; Aki & Richards 2002), which consists of an elastic semi-space bounded by a free-surface boundary condition at $z=0$. This problem is suitable to evaluate the accuracy of the different methods because the results can be compared with the analytic solution. The density, P- and S-wave velocities of the media are given by $\rho=2.5\ \mathrm{g\,cm^{-3}}$, $\alpha=3\ \mathrm{km\,s^{-1}}$ and $\beta=1.73\ \mathrm{km\,s^{-1}}$, respectively, the source is a vertical point force at (0 m, 0.05 km), and there is one receiver on the free surface at (2 km, 0 m). We truncate the domain to a rectangle of 10 km by 3.2 km. The source function is the first derivative of a Gaussian with peak frequency of 17.3 Hz.

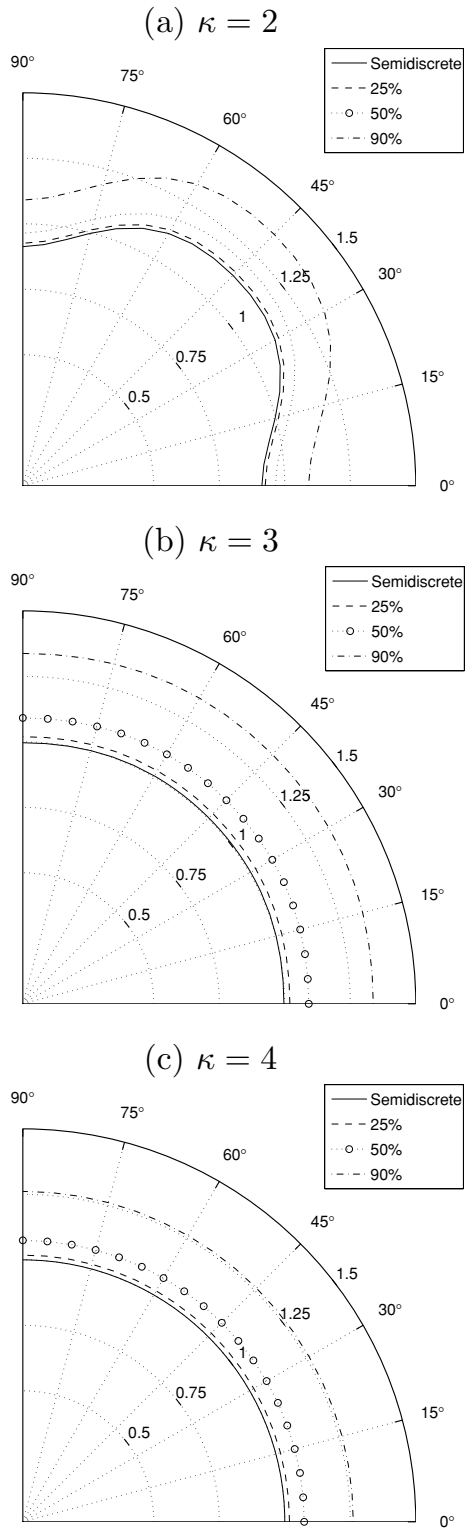

Figure 1. Numerical anisotropy introduced by the grid dispersion using SEM of degrees 2–4, the second order LWM (leap-frog finite differences), $r = 2$ and $\delta = 0.2$ (five gridpoints per wavelength). The dispersion has been magnified for visualization purposes using the following number of wavelengths: (a) 100, (b) 500 and (c) 1000.

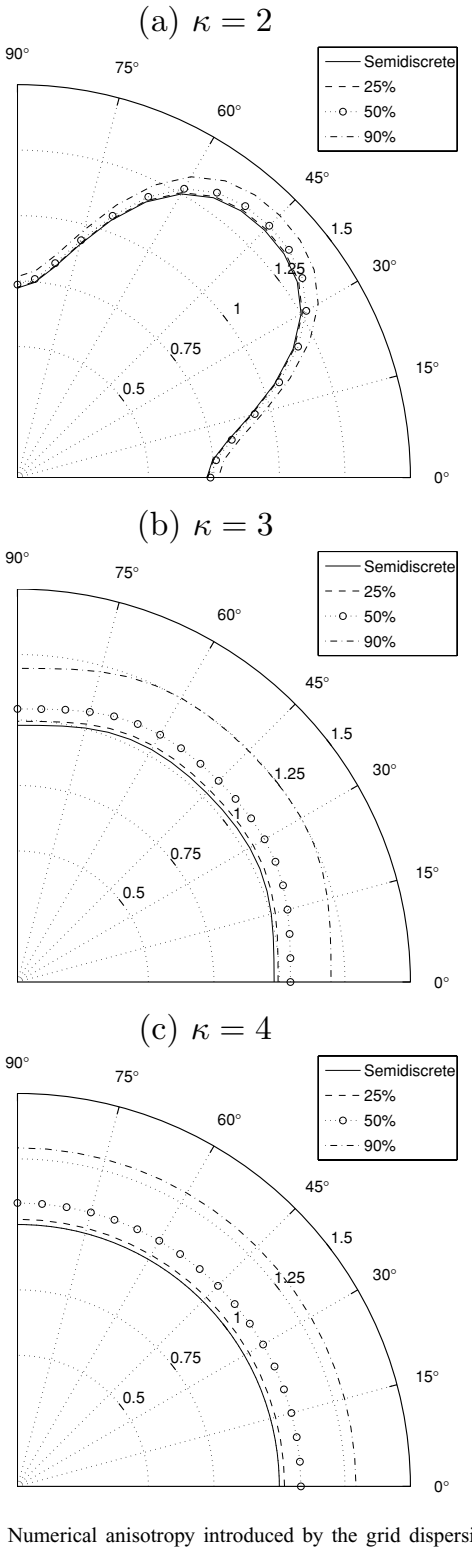

Figure 2. Numerical anisotropy introduced by the grid dispersion using SIPG of degrees 2 to 4, the 2nd order LWM (leap-frog finite differences), $r = 2$ and $\delta = 0.2$. The dispersion has been magnified for visualization purposes using the following number of wavelengths: (a) 300, (b) 3000 and (c) 10 000.

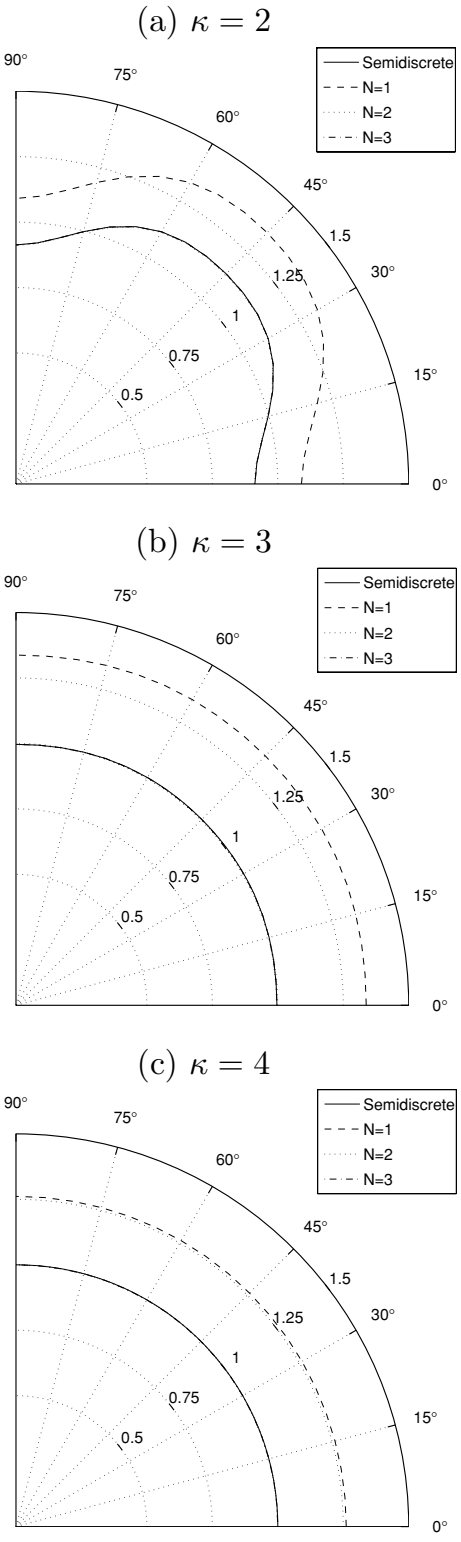

Figure 3. Numerical anisotropy introduced by the grid dispersion using SEM of degrees 2 to 4 and LWM of orders 1 to 3.

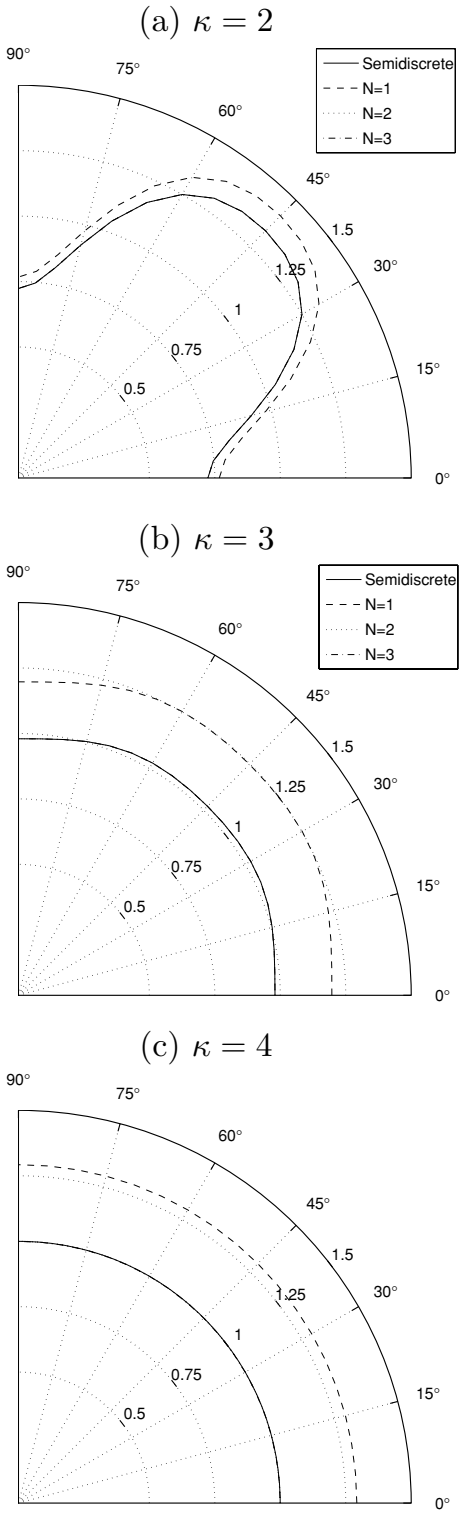

Figure 4. Numerical anisotropy introduced by the grid dispersion using SIPG of degrees 2 to 4 and LWM of orders 1 to 3.

Table 6. Comparison of the RMS error of the seismograms for Lamb's problem (Figs 5–8) using a time step 90, 50 and 25 per cent of the CFL stability condition reported in Table 3 and fourth-degree SEM and IP-DGM.

	SEM				IP-DGM			
	FD2		LW4		FD2		LW4	
(per cent)	Δt	Error	Δt	Error	Δt	Error	Δt	Error
90 per cent	0.00144	4.5×10^{-2}	0.00249	4.1×10^{-2}	0.00053	1.3×10^{-2}	0.00091	1.6×10^{-2}
50 per cent	0.00080	2.1×10^{-2}	0.00139	2.2×10^{-2}	0.00029	8.3×10^{-3}	0.00051	9.8×10^{-3}
25 per cent	0.00040	1.1×10^{-2}	0.00069	1.3×10^{-2}	0.00015	5.6×10^{-3}	0.00025	6.9×10^{-3}

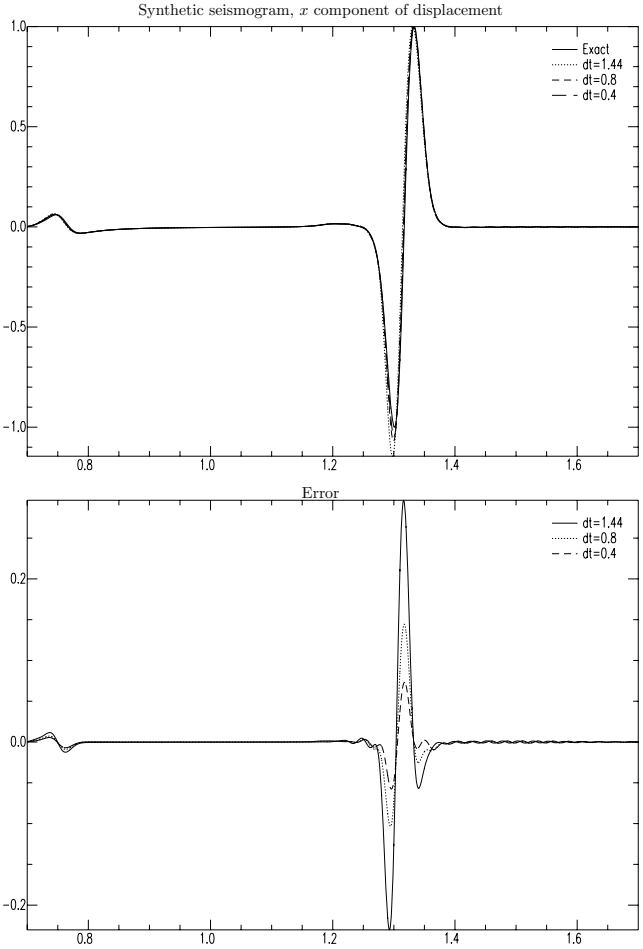

Figure 5. Synthetic seismograms for Lamb's problem using the fourth-degree SEM and the 2nd order FDM.

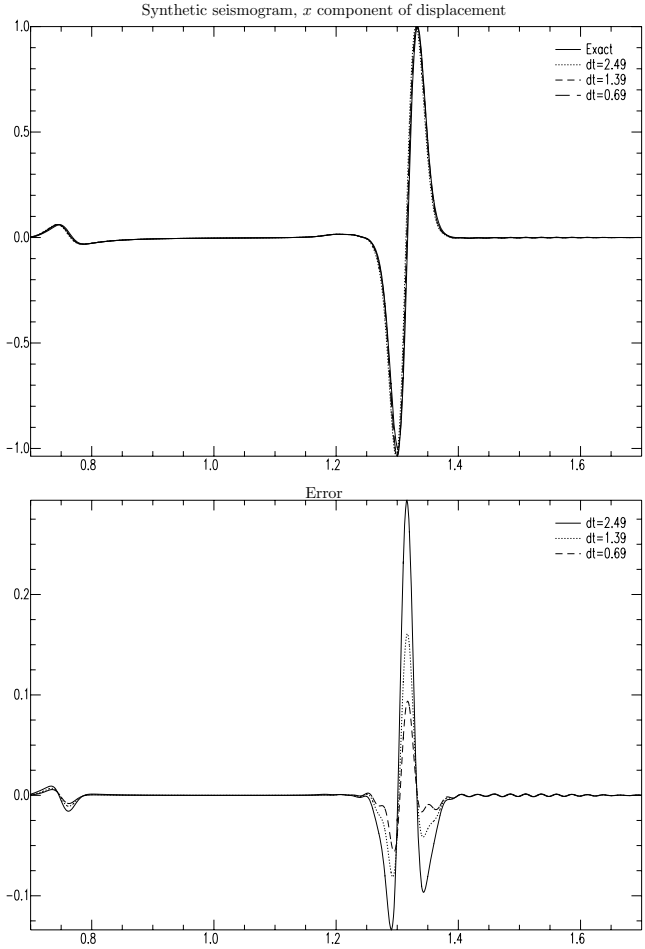

Figure 6. Synthetic seismograms for Lamb's problem using the fourth-degree SEM and the fourth-order LWM.

We compare the accuracy of SEM and IP-DGM using different sizes of time steps and the leap-frog finite difference method (FD2) and the fourth-order Lax-Wendroff method (LW4). We consider time steps that are 90 per cent, 50 per cent and 25 per cent of the stability condition from Table 3, and compare the seismograms with the analytic solution (see Figs 5–8). For the spatial discretization, we use a rectangular mesh of 250 by 80 elements. Using fourth-degree basis functions, this yields a sampling ratio of $\delta = 0.1$, or 10 gridpoints per wavelength, for the S wave. The rms errors are reported in Table 6.

5 CONCLUSIONS

The stability of SEM and IP-DGM was analyzed using LWM for time stepping and a general formulation that allows for high-order basis functions and overcomes the difficulties due to irregular node spacing. We obtained stability conditions that are necessary and sufficient in the acoustic case and for the IP-DGM elastic case, and less than 10 per cent higher than the actual stability limits in the SEM elastic case. The limitation of the analysis is that it assumes regular quadrilateral elements and it does not take into account the boundary conditions. An other restriction is that it was limited to the 2-D case for tensor-product rectangular elements. The following remarks summarize the overall analysis:

(1) The size of the time step is approximately constant with respect to the degree κ if we bound it using the smallest spatial increment (Tables 2 and 4).

(2) IP-DGM requires a time step approximately 20 per cent smaller than that of SEM in the acoustic case, and 60 per cent smaller in the elastic case. This, in addition to the fact that it

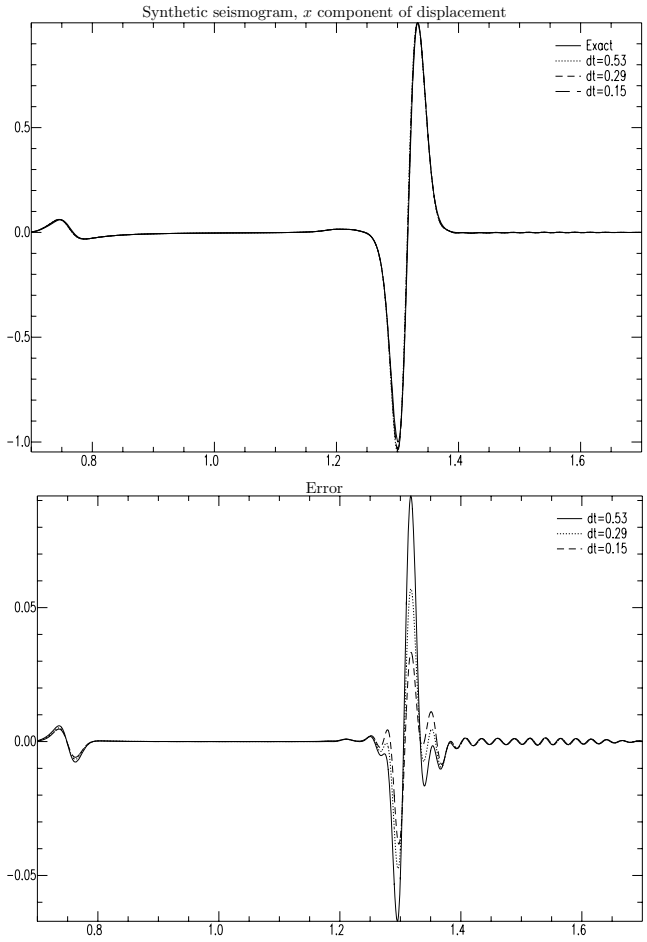

Figure 7. Synthetic seismograms for Lamb's problem using the fourth-degree IP-DGM and the 2nd order FDM.

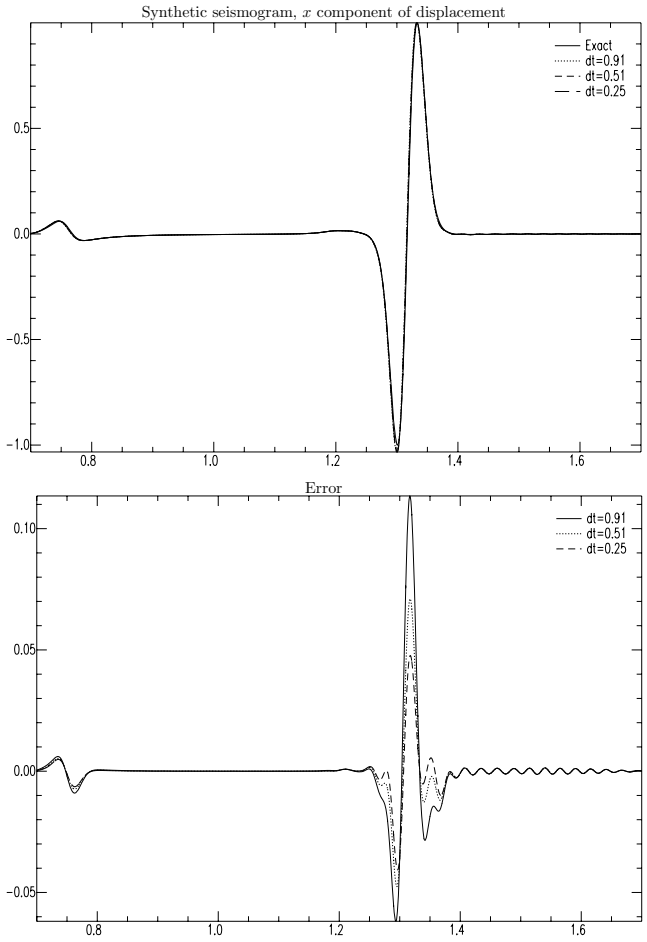

Figure 8. Synthetic seismograms for Lamb's problem using the degree IP-DGM and the fourth-order LWM.

requires more degrees of freedom for a given sampling ratio, makes IP-DGM much more expensive than SEM.

(3) The fourth-order LWM offers double the accuracy with considerably little overhead than the leap-frog FDM since it requires approximately double the operations but allows for a time step 73 per cent higher. The higher-order methods offer an increased accuracy but with a higher computational cost.

We emphasize that IP-DGM is better suited for local refinement and time stepping than SEM (Bey *et al.* 1996; Dumbser *et al.* 2007) (but see Madec *et al.* 2009). Depending on the implementation and on the particular physical problem, these advantages may be used to defray the cost of the reduced time steps.

ACKNOWLEDGMENTS

The authors are grateful to Dimitri Komatitsch and Julien Diaz for their valuable feedback, and to Jean Virieux for his careful review. This work was partially supported by an AEA grant from the King Abdullah University of Science and Technology (KAUST).

REFERENCES

Ainsworth, M., 2004a. Discrete dispersion relation for hp-version finite element approximation at high wave number, *SIAM J. Numer. Anal.,* **42**(2), 553–575.

Ainsworth, M., 2004b. Dispersive and dissipative behaviour of high order discontinuous Galerkin finite element methods, *J. Comput. Phys.* , **198**(1), 106–130.

Ainsworth, M., Monk, P. & Muniz, W., 2006. Dispersive and dissipative properties of discontinuous Galerkin finite element methods for the second-order wave equation, *J. Scient. Comput.,* **27**(1), 5–40.

Aki, K. & Richards, P., 2002. *Quantitative Seismology,* University Science Books, Sausalito, California, 2nd edn.

Arnold, D., Brezzi, F., Cockburn, B. & Marini, L., 2001. Unified Analysis of Discontinuous Galerkin Methods for Elliptic Problems, *SIAM J. Numer. Anal.,* **39**(5), 1749–1779.

Bernacki, M., Lanteri, S. & Piperno, S., 2006. Time-domain parallel simulation of heterogeneous wave propagation on unstructured grids using explicit, nondiffusive, discontinuous Galerkin methods, *J. Comput. Acoust.,* **14**(1), 57–81.

Bey, K., Oden, J. & Patra, A., 1996. A parallel hp-adaptive discontinuous Galerkin method for hyperbolic conservation laws, *Appl. Numer. Math.,* **20**(4), 321–336.

Chaljub, E., Komatitsch, D., Vilotte, J.-P., Capdeville, Y., Valette, B. & Festa, G., 2007. Spectral element analysis in seismology, in *Advances in Wave Propagation in Heterogeneous Media,* pp. 365–419, eds Wu, R.-S. & Maupin, V., Advances in Geophysics, Elsevier.

Chung, E. & Engquist, B., 2006. Optimal discontinuous galerkin methods for wave propagation, *SIAM J. Numer. Anal.,* **44**(5), 2131–2158.

Cockburn, B. & Shu, C., 1989. TVB Runge-Kutta local projection discontinuous galerkin finite element method for conservation laws II: general framework, *Math. Comput.,* **52**(186), 411–435.

Cockburn, B., Lin, S. & Shu, C., 1989. TVB Runge-Kutta local projection discontinuous Galerkin finite element method for conservation laws III: one-dimensional systems, *J. Comput. Phys.,* **84**(1), 90–113.

Cohen, G., 2002. *Higher-Order Numerical Methods for Transient Wave Equations,* Scientific Computation, Springer-Verlag, Berlin.

Dablain, M.A., 1986. The application of high-order differencing to the scalar wave equation, *Geophysics,* **51**(1), 54–66.

Darlow, B., 1980. A Penalty-Galerkin Method for Solving the Miscible Displacement Problem, *PhD thesis*, Rice University, Houston, Texas.

Dawson, C., Sun, S. & Wheeler, M.F., 2004. Compatible algorithms for coupled flow and transport, *Comput. Methods Appl. Mech. Eng.,* **193**(23-26), 2565–2580.

De Basabe, J.D. & Sen, M.K., 2007. Grid dispersion and stability criteria of some common finite-element methods for acoustic and elastic wave equations, *Geophysics,* **72**(6), T81–T95.

De Basabe, J.D., Sen, M.K. & Wheeler, M.F., 2008. The Interior Penalty Discontinuous Galerkin Method for Elastic Wave Propagation: Grid Dispersion, *Geophys. J. Int.,* **175**(1), 83–93.

Diaz, J. & Grote, M., 2009. Energy conserving explicit local time stepping for second-order wave equations, *SIAM J. Scient. Comput.,* **31**(3), 1985–2014.

Dubiner, M., 1991. Spectral methods on triangles and other domains, *J. Scient. Comput.,* **6**(4), 345–390.

Dumbser, M., Käser, M. & Toro, E., 2007. An arbitrary high-order Discontinuous Galerkin method for elastic waves on unstructured meshes—V. Local time stepping and p-adaptivity, *Geophys. J. Int.,* **171**(2), 695–717.

Fauqueux, S., 2003. Eléments finis mixtes spectraux et couches absorbantes parfaitement adaptées pour la propagation d'ondes élastiques en régime transitoire, *PhD thesis*, Université de Paris, IX-Dauphine.

Gilbert, J. & Joly, P., 2008. Higher order time stepping for second order hyperbolic problems and optimal CFL conditions, in *Partial Differential Equations: Modeling and Numerical Simulation,* pp. 67–93, eds Glowinski, R. & Neittaanmäki, P., Computational Methods in Applied Sciences, Springer-Verlag, Berlin.

Grote, M., Schneebeli, A. & Schotzau, D., 2006. Discontinuous Galerkin Finite Element Method for the Wave Equation, *SIAM J. Numer. Anal.,* **44**(6), 2408–2431.

Hu, F.Q., Hussaini, M.Y. & Rasitarinera, P., 1999. An analysis of the discontinuous Galerkin method for wave propagation problems, *J. Comput. Phys.,* **151**(2), 921–946.

Hughes, T.J.R., 2000. *The Finite Element Method,* 2nd edn, Dover Publications, Mineola, New York.

Jund, S. & Salmon, S., 2007. Arbitrary high-order finite element schemes and high-order mass lumping, *Int. J. Appl. Math. Comput. Sci.,* **17**(3), 375–393.

Karniadakis, G. & Sherwin, S., 1999. *Spectral/hp Element Methods for Computational Fluid Dynamics,* Numerical Mathematics and Scientific Computation, Oxford University Press, Oxford.

Käser, M. & Dumbser, M., 2006. An arbitrary high-order discontinuous Galerkin method for elastic waves on unstructured meshes—I. The two-dimensional isotropic case with external source terms, *Geophys. J. Int.,* **166**(2), 855–877.

Komatitsch, D. & Tromp, J., 1999. Introduction to the spectral element method for three-dimensional seismic wave propagation, *Geophys. J. Int.,* **139**(3), 806–822.

Komatitsch, D. & Tromp, J., 2002. Spectral-element simulations of global seismic wave propagation-I. Validation, *Geophys. J. Int.,* **149**(2), 390–412.

Komatitsch, D. & Vilotte, J., 1998. The spectral-element method: an efficient tool to simulate the seismic response of 2D and 3D geological structures, *Bull. seism. Soc. Am.,* **88**(2), 368–392.

Komatitsch, D., Ritsema, J. & Tromp, J., 2002. The spectral-element method, Beowulf computing, and global seismology, *Science,* **298**(5599), 1737–1742.

Komatitsch, D., Tsuboi, S. & Tromp, J., 2005. The spectral-element method in seismology, *Geophysical Monograph,* **157,** 205–227.

Kosloff, D., Filho, A., Tessmer, E. & Behle, A., 1989. Numerical solution of the acoustic and elastic wave equations by a new rapid excpansion method, *Geophys. Prospect.,* **37**(4), 383–394.

Kubatko, E., Westerink, J. & Dawson, C., 2007. Semi discrete discontinuous Galerkin methods and stage-exceeding-order, strong-stability-preserving Runge-Kutta time discretizations, *J. Comput. Phys.,* **222**(2), 832–848.

Lamb, H., 1904. On the propagation of tremors over the surface of an elastic solid, *Phil. Trans. R. Soc. Lond.,* **203,** 1–42.

Lax, P.D. & Wendroff, B., 1964. Difference schemes for hyperbolic equations with high order of accuracy, *Commun. Pure appl. Math.,* **17**(3), 381–398.

Li, B.Q., 2006. *Discontinuous Finite Elements in Fluid Dynamics and Heat Transfer, Computational Fluid and Solid Mechanics,* Springer, London.

Madec, R., Komatitsch, D. & Diaz, J., 2009. Energy-conserving local time stepping based on high-order finite elements for seismic wave propagation across a fluid-solid interface, *Comput. Model. Eng. Sci.,* **49**(2), 163–189.

Marfurt, K.J., 1984. Accuracy of finite-difference and finite-element modeling of the scalar and elastic wave equations, *Geophysics,* **49**(5), 533–549.

Mitchell, A. & Griffiths, D., 1980. *The Finite Difference Method in Partial Differential Equations,* John Wiley and Sons, New York.

Mullen, R. & Belytschko, T., 1982. Dispersion analysis of finite element semidiscretizations of the two-dimensional wave equation, *Int. J. Numer. Methods Eng.,* **18**(1), 11–29.

Nissen-Meyer, T., Fournier, A. & Dahlen, F.A., 2008. A 2-D spectral-element method for computing spherical-earth Seismograms—II. Waves in solid-fluid media, *Geophys. J. Int.,* **174**(3), 873–888.

Patera, A.T., 1984. A spectral element method for fluid dynamics: Laminar flow in a channel expansion, *J. Comput. Phys.,* **54**(3), 468–488.

Priolo, E., 2001. Earthquake Ground Motion Simulation Through the 2-D Spectral Element Method, *J. Computational Acoustics,* **9**(4), 1561–1581.

Rivière, B., 2008. *Discontinuous Galerkin Methods for Solving Elliptic and Parabolic Equations, Theory and Implementation,* SIAM, Philadelphia.

Rivière, B., Wheeler, M. & Girault, V., 1999. Improved energy estimates for interior penalty, constrained and discontinuous Galerkin methods for elliptic problems. Part I, *Computational Geosciences,* **3**(3), 337–360.

Rivière, B., Wheeler, M.F. & Girault, V., 2001. A Priori Error Estimates for Finite Element Methods Based on Discontinuous Approximation Spaces for Elliptic Problems, *SIAM Journal on Numerical Analysis,* **39**(3), 902–931.

Seriani, G. & Priolo, E., 1994. Spectral element method for acoustic wave simulation in heterogeneous media, *Finite Elements in Analysis and Design,* **16**(3-4), 337–348.

Simo, J., Tarnow, N. & Wong, K., 1992. Exact energy-momentum conserving algorithms and symplectic schemes for nonlinear dynamics, *Computer Methods in Applied Mechanics and Engineering,* **100**(1), 63–116.

Tal-Ezer, H., 1986. Spectral methods in time for hyperbolic equations, *SIAM Journal on Numerical Analysis,* **23**(1), 11–26.

Tarnow, N. & Simo, J., 1994. How to render 2nd-order accurate time-stepping algorithms 4th-order accurate while retaining the stability and conservation properties, *Computer Methods in Applied Mechanics and Engineering,* **115**(3-4), 233–252.

Tordjman, N., 1995. Eléments finis d'ordre élevé avec condensation de masse pour l'équation des ondes, *PhD thesis*, Université de Paris, IX-Dauphine.

Tordjman, N., Cohen, G. & Joly, P., 1994. Eléments finis d'ordre élevé avec condensation de masse pour l'équation des ondes en dimension 1, Rapport de Recherche 2323, INRIA, Le Chesnay, France.

Zyserman, F., Gauzellino, P. & Santos, J., 2003. Dispersion analysis of a non-conforming finite element method for the Helmholtz and elastodynamic equations, *International Journal for Numerical Methods in Engineering,* **58**(9), 1381–1395.

APPENDIX A: DGM BASIS FUNCTIONS

In this appendix, we provide a brief summary of the basis functions used in DGM that were considered in this paper. These are the same basis functions that were considered in De Basabe *et al.* (2008), where the reader can find a more detailed description and an analysis of their accuracy. A general description of the basis functions can be found in Hughes (2000) and Karniadakis & Sherwin (1999), and a description of the basis functions used in DGM can be found in Li (2006). An important difference between FEM and DGM is that in

DGM the basis functions are not required to be continuous over the entire domain but only inside the elements. This important feature of DGM implies that the mass matrix is always block-diagonal, which translates in to an efficient time-marching algorithm. Furthermore, the basis functions can be chosen such that the mass matrix is exactly diagonal. In the following, we define three types of basis functions that yield a diagonal mass matrix.

Legendre Basis: The first approach to obtain a diagonal mass matrix is to use tensor products of the Legendre polynomials as the basis functions. These are called modal basis functions (Dubiner 1991; Karniadakis & Sherwin 1999), and it is the traditional approach that has been used in DGM when a diagonal mass matrix is sought (Cockburn & Shu 1989; Cockburn *et al.* 1989; Li 2006). They are orthogonal under the L^2 inner product and have simple recursion formulas for the higher order polynomials and their derivatives. This approach yields a diagonal mass matrix only if the media parameters are constant inside each element.

GLL Basis: A second approach is to use nodal basis functions, making the nodes inside the element match the quadrature points. This idea has been exploited in SEM, where the Gauss-Lobatto-Legendre (GLL) points and quadrature rules are used. This approach leads to a diagonal mass matrix independently of how the media parameters change inside the elements, but the mass matrix integrals are not computed exactly even if the media parameters are piecewise constant.

Gauss Basis: The third approach is closely related to the second one, but uses the Gauss nodes and quadrature rules instead of the GLL nodes and quadrature rules. The primary difference between the Gauss and the GLL nodes is that the endpoints of the interval are always included in the GLL nodes. In this approach, as well as in the second one, the mass matrix is always diagonal but, unlike in the second approach, the integration will be exact for piecewise constant and piecewise linearly varying media parameters.

APPENDIX B: MASS AND STIFFNESS MATRICES

This appendix shows the expressions for the simplified and the dynamic mass and stiffness matrices for the reduced order eigenvalue problem. This has been dealt in detail in De Basabe & Sen (2007) and De Basabe *et al.* (2008) and is summarized here for completeness.

B1 Simplified mass and stiffness matrices

Recall that the analysis assumes that the medium is isotropic, homogeneous, unbounded and source free, that the finite-element mesh is periodic, and that the elements are square with sides parallel to the coordinate axis and with tensor product basis functions (Mullen & Belytschko 1982; Marfurt 1984; Hu *et al.* 1999; Cohen 2002; Zyserman *et al.* 2003; Ainsworth 2004a,b; Ainsworth *et al.* 2006; De Basabe & Sen 2007; De Basabe *et al.* 2008). Introducing the simplifying assumptions in the mass and stiffness matrices yields

(1) Acoustic SEM (compare to eqs 12 and 13)

$$M_{ij} = \left(\phi_j, \phi_i\right)_\Omega, \tag{B1}$$

$$K_{ij} = \mathcal{B}_\Omega(\phi_j, \phi_i). \tag{B2}$$

(2) Elastic SEM (compare to eqs 21 to 25)

$$M_{ij} = (r^2\phi_i, \phi_j)_\Omega, \tag{B3}$$

$$K^1_{ij} = \boldsymbol{\mathcal{B}}_\Omega\left((\phi_j, 0)^T, (\phi_i, 0)^T\right), \tag{B4}$$

$$K^2_{ij} = \boldsymbol{\mathcal{B}}_\Omega\left((0, \phi_j)^T, (\phi_i, 0)^T\right), \tag{B5}$$

$$K^3_{ij} = \boldsymbol{\mathcal{B}}_\Omega\left((\phi_j, 0)^T, (0, \phi_i)^T\right), \tag{B6}$$

$$K^4_{ij} = \boldsymbol{\mathcal{B}}_\Omega\left((0, \phi_j)^T, (0, \phi_i)^T\right), \tag{B7}$$

(3) Acoustic IP-DGM (compare to eqs 30 and 31)

$$M_{ij} = \sum_{E\in\Omega_h} (\varphi_j, \varphi_i)_E \tag{B8}$$

$$K_{ij} = \sum_{E\in\Omega_h} \mathcal{B}_E(\varphi_j, \varphi_i) + \sum_{\gamma\in\Gamma_h} \mathcal{J}_\gamma(\varphi_j, \varphi_i; S, R) \tag{B9}$$

(4) Elastic IP-DGM (compare to eqs 35 to 39)

$$M_{ij} = \sum_{E\in\Omega_h} (r^2\varphi_j, \varphi_i)_E \tag{B10}$$

$$K^1_{ij} = \sum_{E\in\Omega_h} \boldsymbol{\mathcal{B}}_E\left((\varphi_j, 0)^T, (\varphi_i, 0)^T\right) + \sum_{\gamma\in\Gamma_h} \boldsymbol{\mathcal{J}}_\gamma\left((\varphi_j, 0)^T, (\varphi_i, 0)^T\right) \tag{B11}$$

$$K^2_{ij} = \sum_{E\in\Omega_h} \boldsymbol{\mathcal{B}}_E\left((0, \varphi_j)^T, (\varphi_i, 0)^T\right) + \sum_{\gamma\in\Gamma_h} \boldsymbol{\mathcal{J}}_\gamma\left((0, \varphi_j)^T, (\varphi_i, 0)^T\right) \tag{B12}$$

$$K^3_{ij} = \sum_{E\in\Omega_h} \boldsymbol{\mathcal{B}}_E\left((\varphi_j, 0)^T, (0, \varphi_i)^T\right) + \sum_{\gamma\in\Gamma_h} \boldsymbol{\mathcal{J}}_\gamma\left((\varphi_j, 0)^T, (0, \varphi_i)^T\right) \tag{B13}$$

$$K^4_{ij} = \sum_{E\in\Omega_h} \boldsymbol{\mathcal{B}}_E\left((0, \varphi_j)^T, (0, \varphi_i)^T\right) + \sum_{\gamma\in\Gamma_h} \boldsymbol{\mathcal{J}}_\gamma\left((0, \varphi_j)^T, (0, \varphi_i)^T\right) \tag{B14}$$

where

$$\mathcal{B}_E(p, v) = \int_E \nabla p \cdot \nabla v \, \mathrm{d}x \, \mathrm{d}z, \tag{B15}$$

$$\mathcal{J}_\gamma(p, v) = -\int_\gamma \{\nabla p \cdot \boldsymbol{n}^\gamma\}[v] \, d\gamma + S\int_\gamma \{\nabla v \cdot \boldsymbol{n}^\gamma\}[p] \, d\gamma + R\int_\gamma [p][v] \, d\gamma, \tag{B16}$$

$$\boldsymbol{\mathcal{B}}_E(\boldsymbol{u}, \boldsymbol{v}) = \int_E \left((r^2 - 2)\nabla \cdot \boldsymbol{u}\nabla \cdot \boldsymbol{v} + (\nabla \boldsymbol{u} + \nabla \boldsymbol{u}^T) : \nabla \boldsymbol{v}\right) \mathrm{d}x \, \mathrm{d}z, \tag{B17}$$

$$\boldsymbol{\mathcal{J}}_\gamma(\boldsymbol{u}, \boldsymbol{v}) = -\int_\gamma \{(r^2 - 2)u_{k,k}n_i + (u_{i,j} + u_{j,i})n_j\}[v_i] \, d\gamma + S\int_\gamma \{(r^2 - 2)v_{k,k}n_i + (v_{i,j} + v_{j,i})n_j\}[u_i] \, d\gamma + r^2 R\int_\gamma [u_i][v_i] \, d\gamma, \tag{B18}$$

α is the P-wave velocity, β is the S-wave velocity and $r = \alpha/\beta$ is the ratio of the P- to S-wave velocity.

B2 Dynamic mass and stiffness matrices

The dynamic mass and stiffness matrices are computed using the wavenumber and are intrinsically related to plane wave analysis. The procedure to compute the FEM or SEM matrices is involved and takes full advantage of the structure of the tensor product basis functions. In order to give a direct presentation, new notation will be introduced that reflects the tensor-product nature of the basis. As will become evident below, the DGM case is more manageable because the basis functions are defined element wise.

Let us first consider the SEM case. In order to do this, the following notation is introduced to split the indexes of the matrices to take advantage of the tensor product nature:

$$M_{ij} = M_{(i)(j_1,j_2)} \tag{B19}$$

where $j = \kappa\ j_2 + j_1$ and $0 \leq j_1 < \kappa$. Clearly for every j there is a unique pair (j_1, j_2) and vice versa. Furthermore, recall that the analysis assumes an unbounded domain and therefore the matrices are infinite, $-\infty < i, j < \infty$; nevertheless, for a fixed i there is a finite number of non-zero entries because of the local support of the basis functions.

In the acoustic case, the dynamic mass and stiffness matrices are given by

$$\tilde{M}_{(i)(l_1,l_2)} = M_{(i)(\kappa q_1+l_1,\kappa q_2+l_2)} e^{k_x h q_1 + k_z h q_2}, \tag{B20}$$

$$\tilde{K}_{(i)(l_1,l_2)} = K_{(i)(\kappa q_1+l_1,\kappa q_2+l_2)} e^{k_x h q_1 + k_z h q_2}, \tag{B21}$$

for $0 \leq i < \kappa^2$, where $0 \leq l_1, l_2 < \kappa$. Note that summation is implied in the right hand side over q_1 and q_2. Similarly, in the elastic case, the stiffness matrices are given by

$$\tilde{K}^{\nu}_{(i)(l_1,l_2)} = K^{\nu}_{(i)(\kappa q_1+l_1,\kappa q_2+l_2)} e^{k_x h q_1 + k_z h q_2}, \tag{B22}$$

for $\nu = 1, \ldots, 4$.

For IP-DGM, the dynamic mass matrix is identical to the element mass matrix since the global mass matrix is always block diagonal. The dynamic stiffness matrices in the acoustic and elastic cases are as follows:

$$\tilde{K}_{ij} = K_{ij} + e^{-\mathrm{i}k_z h} L^T_{ij} + e^{\mathrm{i}k_z h} L^B_{ij} + e^{-\mathrm{i}k_x h} L^L_{ij} + e^{\mathrm{i}k_x h} L^R_{ij}, \tag{B23}$$

$$\tilde{K}^{\nu}_{ij} = K^{\nu}_{ij} + e^{-\mathrm{i}k_z h} L^{\nu,T}_{ij} + e^{\mathrm{i}k_z h} L^{\nu,B}_{ij} + e^{-\mathrm{i}k_x h} L^{\nu,L}_{ij} + e^{\mathrm{i}k_x h} L^{\nu,R}_{ij}, \tag{B24}$$

where

$$K_{ij} = \mathcal{B}_{\hat{E}}\left(\phi^{\hat{E}}_i, \phi^{\hat{E}}_j\right) + \sum_{f\in\mathcal{S}} \mathcal{J}_{\gamma_f}\left(\phi^{\hat{E}}_j, \phi^{\hat{E}}_i\right), \tag{B25}$$

$$L^f_{ij} = \mathcal{J}_{\gamma_f}\left(\phi^{\hat{E}_f}_i, \phi^{\hat{E}}_j\right), \tag{B26}$$

$$K^1_{ij} = \boldsymbol{\mathcal{B}}_{\hat{E}}\left(\left(\phi^{\hat{E}}_i, 0\right)^T, \left(\phi^{\hat{E}}_j, 0\right)^T\right) + \sum_{f\in\mathcal{S}} \boldsymbol{\mathcal{J}}_{\gamma_f}\left(\left(\phi^{\hat{E}}_i, 0\right)^T, \left(\phi^{\hat{E}}_j, 0\right)^T\right), \tag{B27}$$

$$K^2_{ij} = \boldsymbol{\mathcal{B}}_{\hat{E}}\left(\left(0, \phi^{\hat{E}}_i\right)^T, \left(\phi^{\hat{E}}_j, 0\right)^T\right) + \sum_{f\in\mathcal{S}} \boldsymbol{\mathcal{J}}_{\gamma_f}\left(\left(0, \phi^{\hat{E}}_i\right)^T, \left(\phi^{\hat{E}}_j, 0\right)^T\right), \tag{B28}$$

$$K^3_{ij} = \boldsymbol{\mathcal{B}}_{\hat{E}}\left(\left(\phi^{\hat{E}}_i, 0\right)^T, \left(0, \phi^{\hat{E}}_j\right)^T\right) + \sum_{f\in\mathcal{S}} \boldsymbol{\mathcal{J}}_{\gamma_f}\left(\left(\phi^{\hat{E}}_i, 0\right)^T, \left(0, \phi^{\hat{E}}_j\right)^T\right), \tag{B29}$$

$$K^4_{ij} = \boldsymbol{\mathcal{B}}_{\hat{E}}\left(\left(0, \phi^{\hat{E}}_i\right)^T, \left(0, \phi^{\hat{E}}_j\right)^T\right) + \sum_{f\in\mathcal{S}} \boldsymbol{\mathcal{J}}_{\gamma_f}\left((0, \phi^{\hat{E}}_i)^T, (0, \phi^{\hat{E}}_j)^T\right), \tag{B30}$$

$$L^{1,f}_{ij} = \boldsymbol{\mathcal{J}}_{\gamma_f}\left(\left(\phi^{\hat{E}_f}_i, 0\right)^T, \left(\phi^{\hat{E}}_j, 0\right)^T\right), \tag{B31}$$

$$L^{2,f}_{ij} = \boldsymbol{\mathcal{J}}_{\gamma_f}\left(\left(0, \phi^{\hat{E}_f}_i\right)^T, \left(\phi^{\hat{E}}_j, 0\right)^T\right), \tag{B32}$$

$$L^{3,f}_{ij} = \boldsymbol{\mathcal{J}}_{\gamma_f}\left(\left(\phi^{\hat{E}_f}_i, 0\right)^T, \left(0, \phi^{\hat{E}}_j\right)^T\right), \tag{B33}$$

$$L^{4,f}_{ij} = \boldsymbol{\mathcal{J}}_{\gamma_f}\left(\left(0, \phi^{\hat{E}_f}_i\right)^T, \left(0, \phi^{\hat{E}}_j\right)^T\right), \tag{B34}$$

and $\mathcal{S} = \{T, B, L, R\}$ represent the four surrounding elements from the top, bottom, left and right to the reference element $\hat{E}$.